ECCOMAS Congress 2016
VII European Congress on Computational Methods in Applied Sciences and Engineering
T. Lohner, K. Michaelis, K. Stahl (eds.)
Crete Island, Greece, 5–10 June 2016

LIMITING SHEAR STRESS FORMULATION FOR TEHL SIMULATION

T. Lohner[1], K. Michaelis[1], and K. Stahl[1]

[1] Gear Research Centre (FZG), Technical University of Munich (TUM), Boltzmannstraße 15, 85748 Garching, Germany
e-mail: lohner@fzg.mw.tum.de

Keywords: Elastohydrodynamic lubrication, limiting shear stress, friction, TEHL simulation

Abstract. *Flow curves of typical lubricants show a reduction of lubricant viscosity with increasing shear rate (non-Newtonian fluid behavior). Moreover, measurements of flow curves in pressurized viscometers as well as measurements of friction curves of highly loaded lubricated contacts reveal a limiting value for the shear stress that the lubricant can transmit. This is referred to as the limiting shear stress, at which point visualization of shear bands suggests that internal slip occurs in the lubricant film. It has been shown that the limiting shear stress is not a constant lubricant property, but varies with pressure and temperature. Furthermore, a dependency on the entrainment velocity of the lubricant has been suggested in the literature.*

Many TEHL (thermal elastohydrodynamic lubrication) simulation models have used the viscous Eyring model to describe the non-Newtonian fluid behavior. As the model is not based on a limiting shear stress, the Eyring shear stress and other lubricant property dependencies (e.g. pressure-viscosity) were adjusted to recalculate the measured friction data. However, since this approach appears to be lacking in physical background, visco-plastic models including a limiting shear stress have been introduced. For this, knowledge of the dependencies of the limiting shear stress is required.

This study suggests an expression for the limiting shear stress of lubricants derived from measurements of friction curves at the twin disk test rig. The contact-integral nature of the measurements is adjusted for local use in TEHL simulation models. The limiting shear stress formulation is applied to a finite element (FE) based TEHL simulation model and tested. The non-Newtonian fluid model considered is the simplified Bair/Winer model.

TEHL simulation results achieve very high levels of agreement between the measured and simulated friction curves for a large variety of operating conditions and different lubricants including mineral and synthetic oils. If the sliding velocity is increased further once the maximal friction is reached, it is also possible to quantify the portion of friction reduction that is due to decreasing lubricant viscosity and the portion that is due to the temperature dependency of the limiting shear stress.

1 INTRODUCTION

Newton's law of shear stress for fluid flow describes a linear dependency of shear stress on shear rate with the dynamic viscosity as constant of proportionality. However, flow curves of typical lubricants measured under high pressure exhibit a reduction of lubricant viscosity with increasing shear rate and hence non-Newtonian fluid behavior. Bair [2] [3] measures flow curves in high-pressure rotational viscometers at constant temperature and shows, with increasing shear rate: a linear (Newtonian) regime, a non-linear (shear thinning) regime and a regime of shear-rate-independent shear stress (interpreted as limiting shear stress). A physical interpretation of the latter regime is given by Bair and McCabe [2] [4] observing shear bands with internal slip in fluid flow under high pressure. Thereby, wall slip was not observed. Glass transition is not necessarily accompanied by an occurrence of limiting shear stress (Bair and Winer [8]).

It has been shown that the limiting shear stress is not a constant lubricant property. It is often reported to be a linear function of pressure (Bair [2], Bair and Winer [7], Beilicke et al. [10], Habchi, Bair and Vergne [17]). Bair und Winer [8] show an additional dependency on temperature. Mayer [22] proposes that the limiting shear stress is also subject to variations of entrainment velocity of highly loaded contacts.

The limiting shear stress can either be determined from high-pressure viscometers (primary data measurement) or derived from friction curves measured at tribometers. The former can be limited or very elaborate, particularly at high pressures. For pressures of up to $1000 N/mm^2$, Evans and Johnson [13] show strong correlation between values for the limiting shear stress obtained from a viscometer and values obtained from measured friction curves at the twin disk test rig. The results of a recent research project [24] confirm this for pressures of $> 1000 N/mm^2$. Due to cross-influences between viscous heating and the contact-integral nature of friction curves, the correct interpretation is crucial when deriving limiting shear stresses (Bair [2], Evans and Johnson [13]).

In order to describe the non-Newtonian fluid behavior, functional relationships have been fitted to measured flow curves. A widely used model that does not take into account limiting shear stress, but which presents good numerical practicability (Bartel [9]) has been proposed by Eyring [14]. Bair et al. [5] show that the Eyring model cannot provide a good representation of the shear thinning behavior of lubricants. Furthermore, shear stresses are not limited and can become infinitely large. Models with limiting shear stress have been proposed, e.g. by Bair and Winer [6], Wolff and Kubo [28], and Beilicke et al. [10].

Towards a physically based calculation of highly loaded lubricated contacts, nowadays detailed TEHL simulation programs are used. These programs describe lubricant properties as functions of pressure and temperature as well as of shear rate in terms of viscosity. In this context, Bair et al. [5] notes that the simulation of friction has sometimes turned into a "curve fitting contest" with little consideration of primary measured data.

Wolff and Kubo [28] investigate the influence of different non-Newtonian fluid models by means of isothermal EHL simulations. They recommend the use of limiting-shear-stress-based models and the consideration of thermal effects. Habchi [16] also emphasizes the importance of taking into account thermal effects, based on TEHL simulations with a modified Carreau-Yasuda model [1]. As the Carreau-Yasuda model does not limit the shear stress, it has been truncated numerically based on a linear pressure dependency of the limiting shear stress. Based on the Eyring model, Bobach et al. [11] obtain very strong correlation between TEHL simulation results and measured friction curves from the FZG twin disk test rig. Based on the same TEHL simulation model and a combined Eyring and simplified Bair/Winer model, Beilicke et al. [10] again achieve very strong correlation between simulated and measured

friction curves. In these studies, the limiting shear stress is described as linearly dependent on pressure and derived from measurements at a twin disk test rig.

This paper suggests an expression for the limiting shear stress of lubricants derived from measurements of friction curves at the FZG twin disk test rig. One mineral oil (MIN100), two polyalphaolefine oils (PAO10 and PAO100) and one polyglycol oil (PG100) are considered. The contact-integral nature of the measurements is adjusted for local use in TEHL simulation models. The limiting shear stress formulation is applied to a finite element (FE) based TEHL simulation model as described by Lohner et al. [21] and tested by means of a non-Newtonian fluid model based on the simplified Bair/Winer model (Wolff and Kubo [28]). TEHL simulation results show very high levels of agreement between measured and simulated friction curves for a large variety of operating conditions and for the different types of lubricants considered. If the sliding velocity is increased further once the maximal friction is reached, it is also possible to quantify the portion of friction reduction that is due to decreasing lubricant viscosity and the portion that is due to the temperature dependency of the limiting shear stress.

2 LIMITING SHEAR STRESS FORMULATION

The proposed limiting shear stress formulation for implementation in TEHL simulation models has its origin in a contact-integral approach, which is further developed to a contact-local approach. The work in this section is supported by student coursework by Paschold [23], performed with guidance from the author.

The contact-integral approach $\tau_{\lim|exp}$ is derived from measurements of friction curves at the FZG twin disk test rig and consists of the sum of three terms as given by Eq. (1). The lubricant-specific parameters $E_{\dot{\gamma}1}$, $E_{\dot{\gamma}2}$, $E_{\dot{\gamma}3}$ und $E_{\dot{\gamma}4}$ are obtained from regression analysis. $\tau_{\lim|exp}$ is then transferred to a contact-local approach $\tau_{\lim|sim}$ acc. to Eq. (2).

$$\tau_{lim|exp}(p_m, v_\Sigma, T_{ref}) = E_{\dot{\gamma}1} \cdot \mathrm{p_m} + \left[E_{\dot{\gamma}2} + E_{\dot{\gamma}3} \cdot \ln\left(\mathrm{v_\Sigma} \cdot 1\frac{s}{m}\right)\right] + E_{\dot{\gamma}4} \cdot T_{ref} \tag{1}$$

$$\tau_{lim|sim}(p, v_\Sigma, T_{ref}, T) = \begin{cases} \tau_{lim,m} & f\ddot{u}r\ \tau_{lim|sim} \leq \tau_{lim,m} \\ \frac{4}{\pi} \cdot \tau_{\lim|exp}(p_m = p, v_\Sigma, T_{ref}) \cdot sinh\left(\frac{T_{ref}}{T}\right) & f\ddot{u}r\ \tau_{lim|sim} > \tau_{lim,m} \end{cases} \tag{2}$$

The workflow for deriving $\tau_{lim|sim}$ and the lubricant-specific parameters $E_{\dot{\gamma}1}$, $E_{\dot{\gamma}2}$, $E_{\dot{\gamma}3}$ and $E_{\dot{\gamma}4}$ is schematically shown in Figure 1. The starting point features measured friction curves, whose behavior resembles that of flow curves obtained from high pressure viscometers (see section 1). They typically present a linear (Newtonian) regime, a non-linear (shear thinning) regime and a regime of maximal or rather decreasing friction (see a and b in Figure 1). For mild operating conditions, no maximum of friction may be observed for the considered range of sliding velocity v_g (see c in Figure 1). Due to the increasing bulk (T_M) and TEHL contact temperature as v_g increases, the friction curves become dominated by thermal effects.

2.1 Contact-integral approach

A maximum of the measured friction curves is interpreted as some integral value $\tau_{lim|exp}$ for the limiting shear stress. Therefore, for all friction curves featuring a maximum, the values of p_m, v_Σ, T_M, T_{Oil} and $\tau_{lim|exp}$ are evaluated (see Figure 1 left), whereby $\tau_{lim|exp}$ is obtained from the ratio of friction force F_R and Hertzian contact area A_H. Mayer [22] measured friction curves for different lubricants in the fluid film lubrication regime over a large range of operat-

ing conditions ($p_H = \{600|1200\} N/mm^2$, $\vartheta_{Oil} = \{40|100\}°C$, $v_\Sigma = \{1 \dots 16\} m/s$, $v_g = \{0 \dots 5.33\} m/s$) at the FZG twin disk test rig with cylindrical disks with polished surfaces. Four selected lubricants from Mayer [22] - MIN100, PAO100, PAO10 and PG100 - are considered in this study. The measured kinematic viscosities ν at $40°C$ und $100°C$ are shown in Table 1. Further lubricant data is documented by Mayer [22] and ITR Clausthal [19].

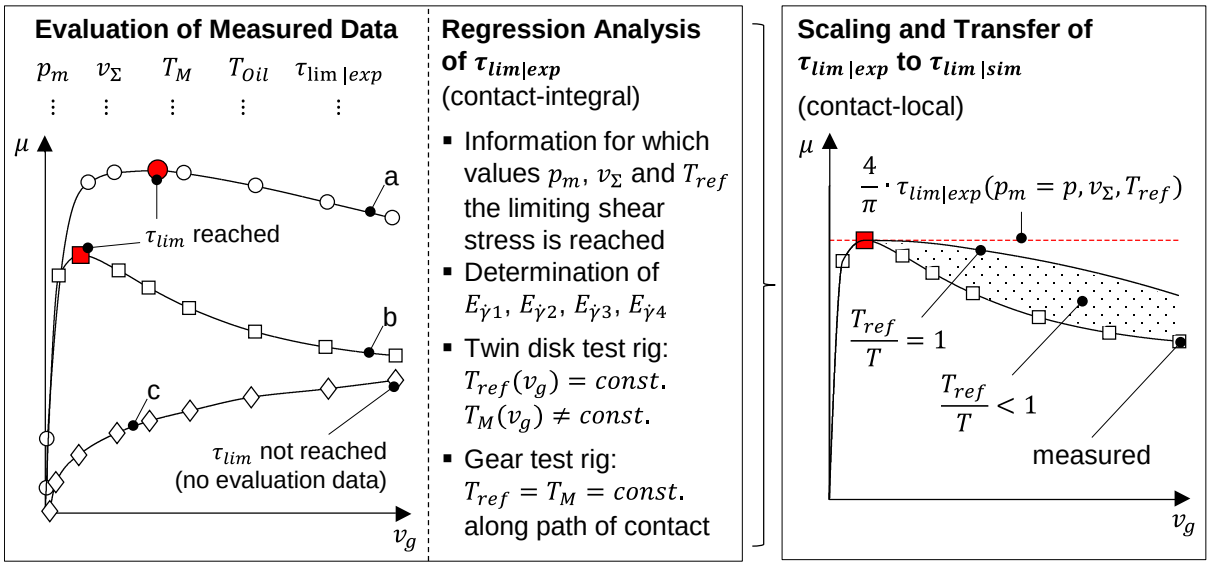

Figure 1: Workflow for determination of contact-integral limiting shear stress $\boldsymbol{\tau_{lim|exp}}$ and its scaling and transfer to a contact-local approach $\boldsymbol{\tau_{lim|sim}}$

Kinematic viscosity	**MIN 100**	**PAO100**	**PAO10**	**PG100**
$\nu(40°C)\ in\ mm^2/s$	95.0	104.6	63.7	99.4
$\nu(100°C)\ in\ mm^2/s$	10.0	15.5	9.9	18.0

Table 1: Measured kinematic viscosities of the considered lubricants (Mayer [22])

Figure 2 exemplifies the measured friction curves for MIN100 and PG100, with two operating conditions (low and high load).

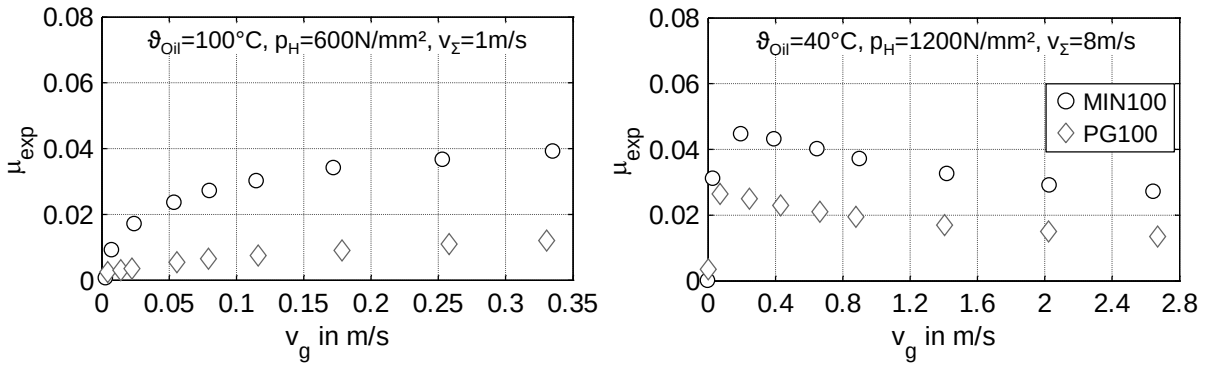

Figure 2: Measured friction curves at the FZG twin disk test rig (exemplarily, measured data acc. to Mayer [22])

Based on the measured friction curves of Mayer [22], Figure 3 shows the evaluated values of $\tau_{lim\,|exp}$ plotted over p_m, v_Σ und T_M for the four selected lubricants MIN100, PAO100, PAO10 and PG100.

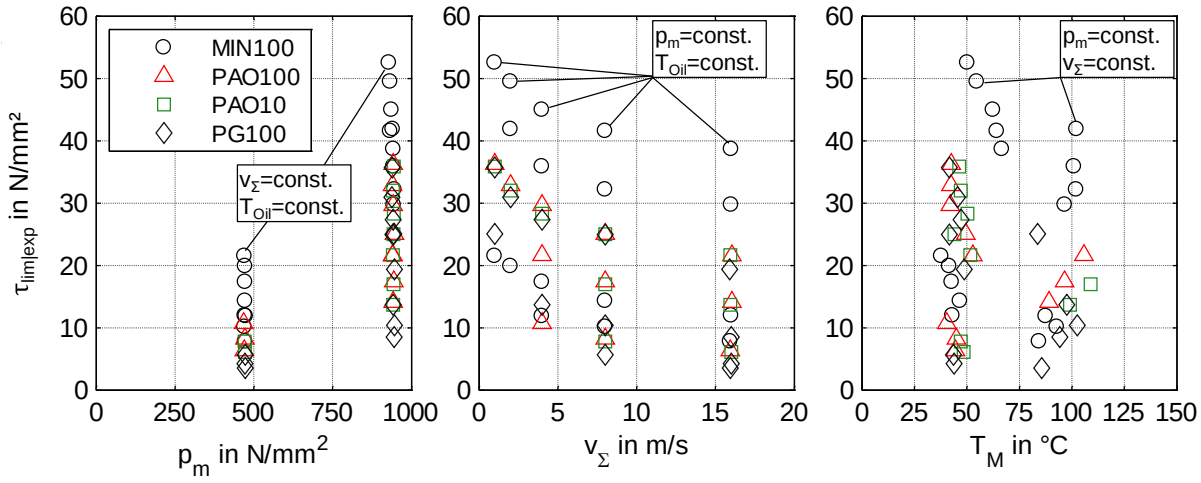

Figure 3: Contact-integral limiting shear stress values $\boldsymbol{\tau_{lim\,|exp}}$ derived from measured friction curves at the FZG twin disk test rig plotted over $\boldsymbol{p_m}$, $\boldsymbol{v_\Sigma}$ and $\boldsymbol{T_M}$ (measurement data acc. to Mayer [22])

Thereby, the following functional relationships of $\tau_{\lim\,|exp}$ with respect to p_m, v_Σ and T_M can be employed:

- $\tau_{lim\,|exp}(p_m) = E_{\dot{\gamma}1} \cdot p_m$ (see Bair [2], Bair und Winer [7], Beilicke et al. [10] and Habchi, Bair und Vergne [17])
- $\tau_{lim\,|exp}(v_\Sigma) = E_{\dot{\gamma}2} + E_{\dot{\gamma}3} \cdot ln(v_\Sigma)$ (see Mayer [22])
- $\tau_{lim\,|exp}(T_{ref} = T_M) = E_{\dot{\gamma}4} \cdot T_{ref}$

As no useable relationship for $\tau_{lim\,|exp}(T_{ref} = T_M)$ has been found in the literature and as only two measurement levels specified by T_{Oil} are available, a simplified linear function is chosen. The bulk temperature T_M is a system-related quantity of the FZG twin disk test rig and increases depending on the operating condition more or less with increasing sliding velocity v_g. Therefore, only T_M at maximal friction (see Figure 1 left) is considered and denoted as reference temperature T_{ref}. Strictly speaking, T_{ref} (and T_M) is not a contact-integral value but more a "boundary condition" of the temperature level of the TEHL contact. However, for almost all derived limiting shear stresses $\tau_{lim\,|exp}$ the amount by which the TEHL contact temperature exceeds T_M is low and comparable, so that T_{ref} can be interpreted as a contact-integral quantity. For the FZG twin disk test rig, it was found that T_{ref} can be well-approximated by a function of p_m, v_Σ and T_{Oil}. This however is not representative of other tribological systems. For gears, T_M is approximately constant over the path of contact, i.e. $T_{ref} = T_M \neq f(p_m, v_\Sigma)$.

The simple operation of adding together the single functional relationships of $\tau_{lim\,|exp}$ in Eq. (1) yields very strong correlation with measured $\tau_{lim\,|exp}$ values (Figure 4 left). Thereby, the lubricant-specific parameters $E_{\dot{\gamma}1}$, $E_{\dot{\gamma}2}$, $E_{\dot{\gamma}3}$ und $E_{\dot{\gamma}4}$ shown in Table 2 are obtained from regression analysis based on Eq. (1). A comparison of the regression quality of the proposed relationship ($\tau_{lim|exp}(p_m, v_\Sigma, T_{M,sys})$, Figure 4 left) with a frequently used linear pressure-dependent relationship ($\tau_{lim|exp}(p_m)$, Figure 4 right) illustrates that the latter is not sufficient.

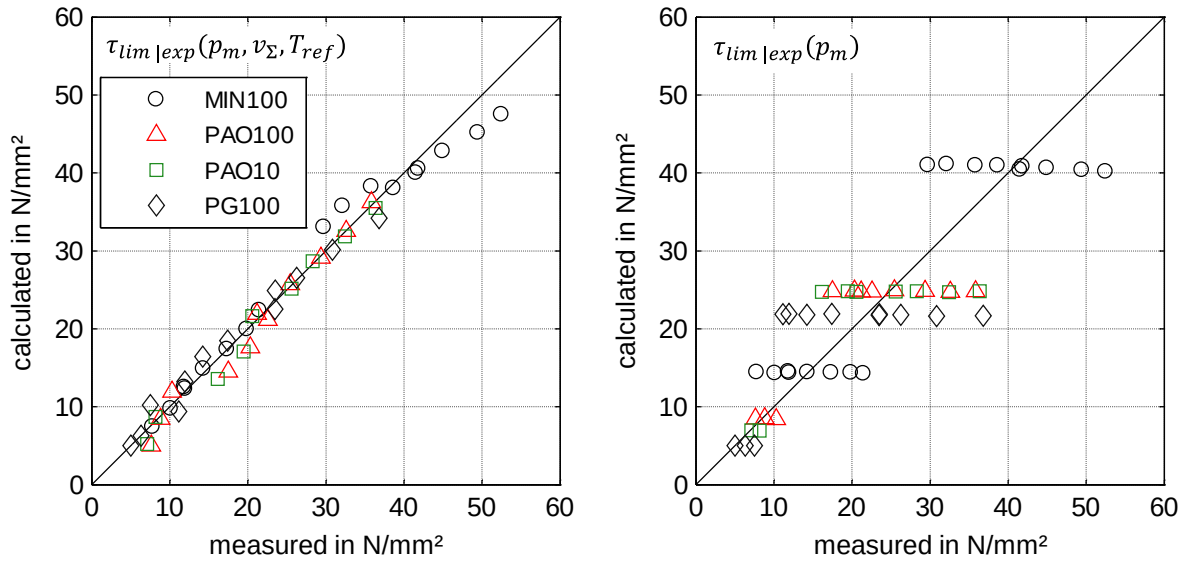

Figure 4: Regression quality of contact-integral limiting shear stress for the proposed relationship $\boldsymbol{\tau_{lim|exp}(p_m, v_\Sigma, T_{M,sys})}$ (left) and the relationship $\boldsymbol{\tau_{lim|exp}(p_m)}$ (right) frequently used in the literature

	MIN 100	**PAO100**	**PAO10**	**PG100**
$E_{\dot{\gamma}1}$	0.0588	0.0376	0.0351	0.0287
$E_{\dot{\gamma}2}\ in\ N/m^2$	32.08	50.21	48.94	70.41
$E_{\dot{\gamma}3}\ in\ N/m^2$	−3.352	−4.770	−4.876	−5.136
$E_{\dot{\gamma}4}\ in\ N/m^2/K$	−0.1195	−0.1564	−0.1455	−0.2005

Table 2: Lubricant-specific parameters of contact-integral limiting shear stress $\tau_{lim\,|exp}$ derived from friction curves

2.2 Contact-local approach

The contact-integral approach $\tau_{lim|exp}(p_m, v_\Sigma, T_{M,sys})$ presented in Eq. (1) is so far only based on evaluated friction curve measurements. In the next step, it is further developed to the contact-local approach $\tau_{lim\,|sim}(p, v_\Sigma, T_{ref}, T)$ in Eq. (2) (see Figure 1 right).

First, p_m is replaced by the local pressure p in the TEHL contact and $\tau_{lim\,|sim}$ is scaled by a factor of $4/\pi$. The latter is required due to the contact-integral nature of $\tau_{lim\,|exp}$ and may be somehow related to the relation $p_H = 4/\pi \cdot p_m$. Example TEHL simulations have shown that the scaling factor of $4/\pi$ provides a very good match for the level of measured friction coefficients for different types of lubricants. Second, a relative temperature dependency of the limiting shear stress is introduced by relating the reference temperature T_{ref} to the local temperature T in the TEHL contact. Hence, $\tau_{lim\,|sim}(p, v_\Sigma, T_{ref}, T)$ becomes a non-linear quantity that varies over the film thickness length (z) and height direction (x). It will be shown that the decrease of friction curves after the maximal friction (see a and b in Figure 1) is partly due to decreasing viscosity and partly due to decreasing limiting shear stress. The *sinh* function provides very good match for the temperature-dependent decrease of the limiting shear stress[1].

[1] The Eyring model is also based on the *sinh* function. As Eyring [14] derived his model from measurements at a capillary viscometer where a proper separation of shear thinning and thermal effects is not possible (Bair et al. [5]), some relation between the temperature dependency of $\tau_{lim\,|sim}$ and primary measured data may be assumed.

A limiting shear stress less than or equal to zero is meaningless. Hence, the minimal value of $\tau_{lim\,|sim}(p, v_\Sigma, T_{ref}, T)$ is generally set to $\tau_{lim,m} = 5N/mm^2$.

2.3 Assumptions

The proposed limiting shear stress formulation for implementation in TEHL simulation models is subject to some assumptions:

- The derived and assumed functional relationships of $\tau_{\lim|exp}$ with respect to p_m, v_Σ and T_{ref} are representative.
- The dependency of $\tau_{lim|exp}$ on the contact-integral quantity p_m is representative for the contact-local quantity p.
- T_{ref} is an appropriate reference value for the temperature dependency of $\tau_{lim|sim}$. The (inevitable) error when calculating T_{ref}/T (T_{ref} represents a bulk temperature) is small and similar for different operating conditions.
- The sum velocity v_Σ influences $\tau_{lim|exp}$ [2] directly.

3 TEHL CALCULATION

The TEHL simulation model used is based on a complete FE implementation and described in detail by Lohner et al. [21]. Only the main characteristics of the model and lubricant properties are repeated here. For simplification, a line contact model is considered.

3.1 TEHL simulation model

The fluid flow is described by the transient generalized Reynolds equation, whereas the elastic deformation of the equivalent body is obtained by solving the linear elasticity equation. For constant temperature, Reynolds, elasticity and load balance equations are solved within a FEM-model(P,H) based on the full-system approach of Habchi [16] achieving very high convergence rates without requiring underrelaxation. For constant pressure and film thickness, the temperature distribution in lubricant and solids is calculated within a FEM-model($\bar{T}$) by solving the corresponding energy equations, which are also based on FE discretization. An iterative procedure is established between the FEM-model(P,H) and FEM-model($\bar{T}$) until the maximum absolute difference of two consecutive solutions of pressure and temperature is smaller than 10^{-3}. The coefficient of friction $\mu_{f|sim}$ of the TEHL contact is evaluated by integrating the shear stress in the middle of the lubricant film:

$$\mu_{f|sim} = \frac{\int_{x_{in}}^{x_{ex}} \tau_{fzx}\big|_{z=\frac{h}{2}} dx}{F_N / l_{eff}} \tag{3}$$

3.2 Temperature and pressure dependency of lubricant properties

The temperature and pressure dependency of the viscosity is defined as suggested by Hepermann et al. [18]. The temperature dependency of the dynamic viscosity at ambient pressure $\eta(T)$ is described acc. to Vogel [27], Fulcher [15] and Tammann and Hesse [26]:

[2] It is also conceivable that v_Σ is only a quantity representing the influence of relaxation time (contact time) or the influence of lubricant film formation on the formation of shear bands.

$$\eta(T) = A_\eta \cdot exp\left(\frac{B_\eta}{C_\eta + (T - 273.15K)}\right) \tag{4}$$

The pressure dependency of the viscosity at a given temperature $\eta(T,p)$ is modelled acc. to Roelands [25]

$$\eta(T,p) = \eta(T) \cdot exp\left\{(ln(\eta(T)) + 9.67) \cdot \left[-1 + \left(1 + \frac{p}{p_{\eta 0}}\right)^{z_\eta(T)}\right]\right\} \tag{5}$$

with a temperature-dependent pressure exponent $z_\eta(T)$ acc. to

$$z_\eta(T) = \frac{\alpha_p(T) \cdot p_{\eta 0}}{\ln(\eta(T)) + 9.67} \tag{6}$$

and a temperature-dependent pressure-viscosity coefficient $\alpha_p(T)$ acc. to

$$\alpha_p(T) \ = E_{\alpha_p 1} \cdot exp\left(E_{\alpha_p 2} \cdot T\right). \tag{7}$$

The temperature and pressure dependency of lubricant density $\rho_f(T,p)$ is modelled following the Bode model [12]:

$$\rho_f(T,p) = \frac{\rho_s \cdot (1 - \alpha_s \cdot T)}{1 - D_{\rho 0} \cdot ln\left(\frac{D_{\rho 1} + D_{\rho 2} \cdot T + D_{\rho 3} \cdot T^2 + p}{D_{\rho 1} + D_{\rho 2} \cdot T + D_{\rho 3} \cdot T^2}\right)} \tag{8}$$

All model constants of the lubricant models above have been obtained from regression of measurements provided by ITR Clausthal [19]. The temperature and pressure dependency of the thermal conductivity $\lambda_f(p)$ and heat capacity per volume $(c_{p,f} \cdot \rho_f)(T,p)$ are based on the models of Larsson and Andersson [20]. Thereby, different parameters are available for different types of lubricant.

3.3 Non-Newtonian fluid behavior

The non-Newtonian fluid behavior is based on the simplified Bair/Winer model (Wolff and Kubo [28]), which can generally be written as:

$$\dot{\gamma}_{\mathrm{fzx}} = \frac{1}{G} \cdot \frac{d\tau_{fzx}}{dt} + \frac{\tau_{fzx}}{\eta(T,p)} \cdot \frac{1}{\left(1 - \left|\frac{\tau_{fzx}}{\tau_{\lim|sim}}\right|\right)} \ \ with \ \tau_{fzx}(T,p,\dot{\gamma}_{fzx}) = \eta(T,p,\dot{\gamma}_{fzx}) \cdot \dot{\gamma}_{fzx} \tag{9}$$

Wolff and Kubo [28] show that the visco-elastic term mainly influences friction for very small slip ratios. Therefore and due to unknown values of the shear modulus, the visco-elastic term is neglected ($G = \infty$) for the sake of simplicity.

4 RESULTS AND DISCUSSION

In the following, simulated values for the coefficients of friction $\mu_{f|sim}$ are compared with measured values μ_{exp} given by Mayer [22] (see section 2.1) for a large variety of operating conditions and for the lubricants MIN100, PAO100, PAO10 and PG100.

Figure 5 exemplifies the simulated and measured friction curves for MIN100 and PG100, with two different operating conditions (see also Figure 2). The measured coefficients of friction very strongly agree with the full-potential TEHL simulation results (thermal, $\sinh(T_{ref}/$

T) acc. to Eq. (2), solid lines)[3]. Deviations can in particular be recognized at the beginning of the friction curves at the non-linear (shear thinning) transition regime. Even though these zones of the friction curves require a higher measurement resolution for systematic comparisons, these deviations could possibly be due to neglected visco-elastic effects ($G = \infty$ in Eq. (9)) and an inaccurate representation of shear thinning by Eq. (9). Furthermore, the overestimation of the coefficient of friction at beginning of the friction curves for MIN100 appears to be correlated with the strong increase of the viscosity of MIN100 with pressure measured by ITR Clausthal [19]. In this context, stationary viscosity measurements at high pressure viscometers may be not simply transferable to TEHL contacts featuring very low contact times.

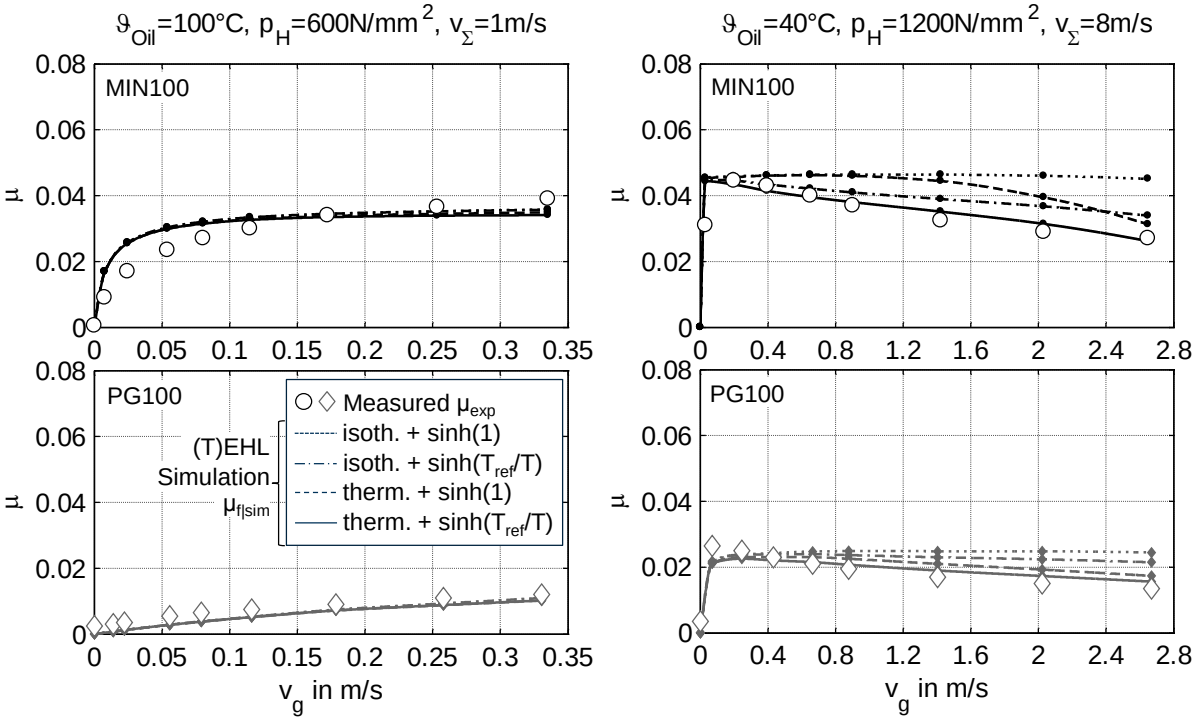

Figure 5: Comparison of simulated ($\boldsymbol{\mu_{f|sim}}$) and measured ($\boldsymbol{\mu_{exp}}$) coefficients of friction for two different operating conditions and for lubricants MIN100 and PG100 (measured data acc. to Mayer **[22]**)

In order to quantify the complex relationship of the influences on the simulated coefficients of friction, simulation results with decreasing level of detail are provided in Figure 5. As its effects are best recognizable for the operating condition with $p_H = 1200N/mm^2$, $\vartheta_{Öl} = 40°C$ and $v_\Sigma = 8m/s$, the following explanations are focused on that.

When thermal effects and the relative temperature dependency of $\tau_{\lim|sim}$ (isothermal, $sinh(1)$ in Eq. (2), dotted lines) are deactivated, the friction curves are almost constant as the sliding velocity v_g increases. Despite $\tau_{\lim|sim}(v_g) = const$, there is a small decrease at high values of v_g caused by shear thinning effects (Habchi, Bair und Vergne [17]). When thermal effects (thermal, sinh(1) in Eq. (2), dashed lines) are activated, a comparatively large decrease in $\mu_{f|sim}$ can be observed. This is mainly due to viscous heating and the corresponding reduction of integral viscosity. The remaining difference in μ_{exp} is a result of the temperature de-

[3] The simulations are exclusively conducted for the measurement points of Mayer [22] (nine measurement points for each friction curve, in-between interpolated for the sake of presentation). The measured bulk temperature of each measurement point serves as boundary condition of the TEHL simulation model.

pendency of $\tau_{lim|sim}$ (isothermal, $\sinh(T_{ref}/T)$ in Eq. (2), dot-dashed lines). The effects of the individual influences depend significantly on the bulk and TEHL contact temperatures, interact mutually and cannot simply be summed together.

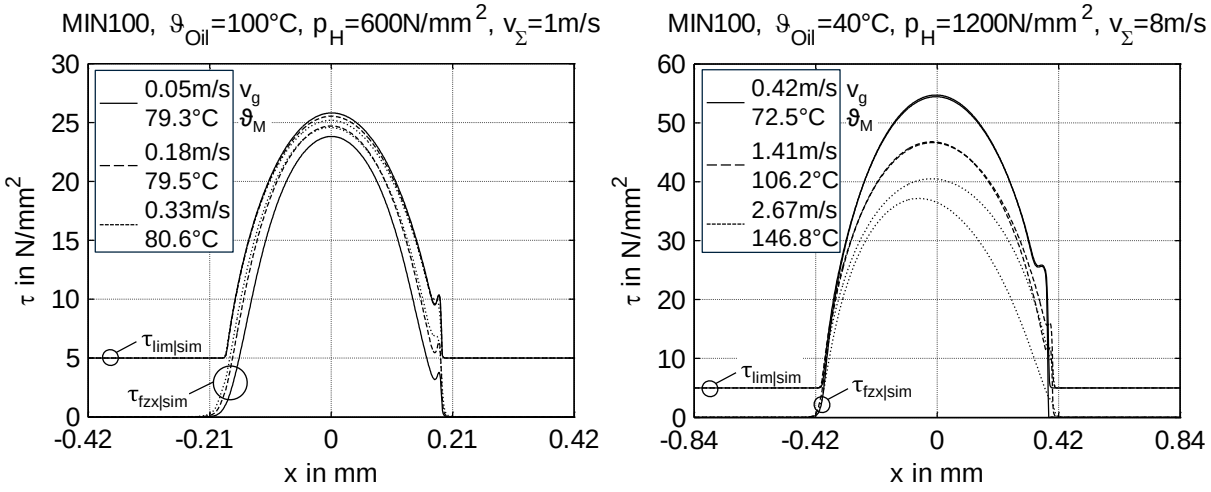

Figure 6: Contact-local shear stress ($\boldsymbol{\tau_{fzx|sim}}$) and limiting shear stress ($\boldsymbol{\tau_{lim\,|sim}}$) distributions in the middle of the lubricant film thickness ($\boldsymbol{z = h/2}$) for MIN100 and selected operating conditions in **Figure 5**

Figure 6 exemplifies the contact-local distributions of the shear stress $\tau_{fzx|sim}$ and limiting shear stress $\tau_{lim\,|sim}$ at the midpoint of the lubricant film thickness ($z = h/2$) for MIN100, with the operating conditions selected in Figure 5 (full-potential TEHL simulation results). The contact-local behavior of $\tau_{lim\,|sim}$ is acc. to Eq. (2) determined by its dependency on the local quantities p and T. This also means that $\tau_{lim\,|sim}$ may only be achieved at specific locations in the TEHL contact. Figure 6 (right) demonstrates again on a contact-local basis that the decrease of the friction curves after a maximal friction value is partly due to decreasing limiting shear stress and partly due to decreasing viscosity with increasing TEHL contact temperature: For the low and medium sliding velocity of $v_g = \{0.42|1.41\} m/s$, $\tau_{lim\,|sim}$ is reached for almost the whole contact area, whereas for the high sliding velocity of $v_g = 2.67 m/s$, $\tau_{fzx|sim}$ is significantly lower than $\tau_{lim\,|sim}$. For the low load operating condition in Figure 6 (left), $\tau_{lim\,|sim}$ is not reached at all for the whole contact area. Moreover, $\tau_{lim\,|sim}$ is almost equal for all sliding velocities, because its relative temperature dependency has almost no influence, due to the low TEHL contact temperatures. Nevertheless, $\tau_{lim\,|sim}$ determines the level of the coefficient of friction.

In summary, Figure 7 shows a comparison of the simulated ($\mu_{f|sim}$) and measured (μ_{exp}) coefficients of friction for all investigated operating conditions of Mayer [22]. It can be seen that the simulated values for the coefficients of friction based on the introduced limiting shear stress formula in section 2 and the non-Newtonian fluid behavior in section 3.3 correlate very strongly with the measured values over a large spread of operating conditions and different types of lubricants. In order to assign the symbols in Figure 7 to the "position" on the friction curves, the symbols are colored proportionally to the slip ratio. Most of the symbols with poor correlation between $\mu_{f|sim}$ and μ_{exp} show very low slip ratios and are therefore located at the beginning of the friction curves. Reasons for this have already been discussed above. It should be mentioned that for some friction curves of PAO10 small solid load portions and therefore

mixed lubrication regimes are not precluded. This has however so far not been considered in the presented TEHL simulation model.

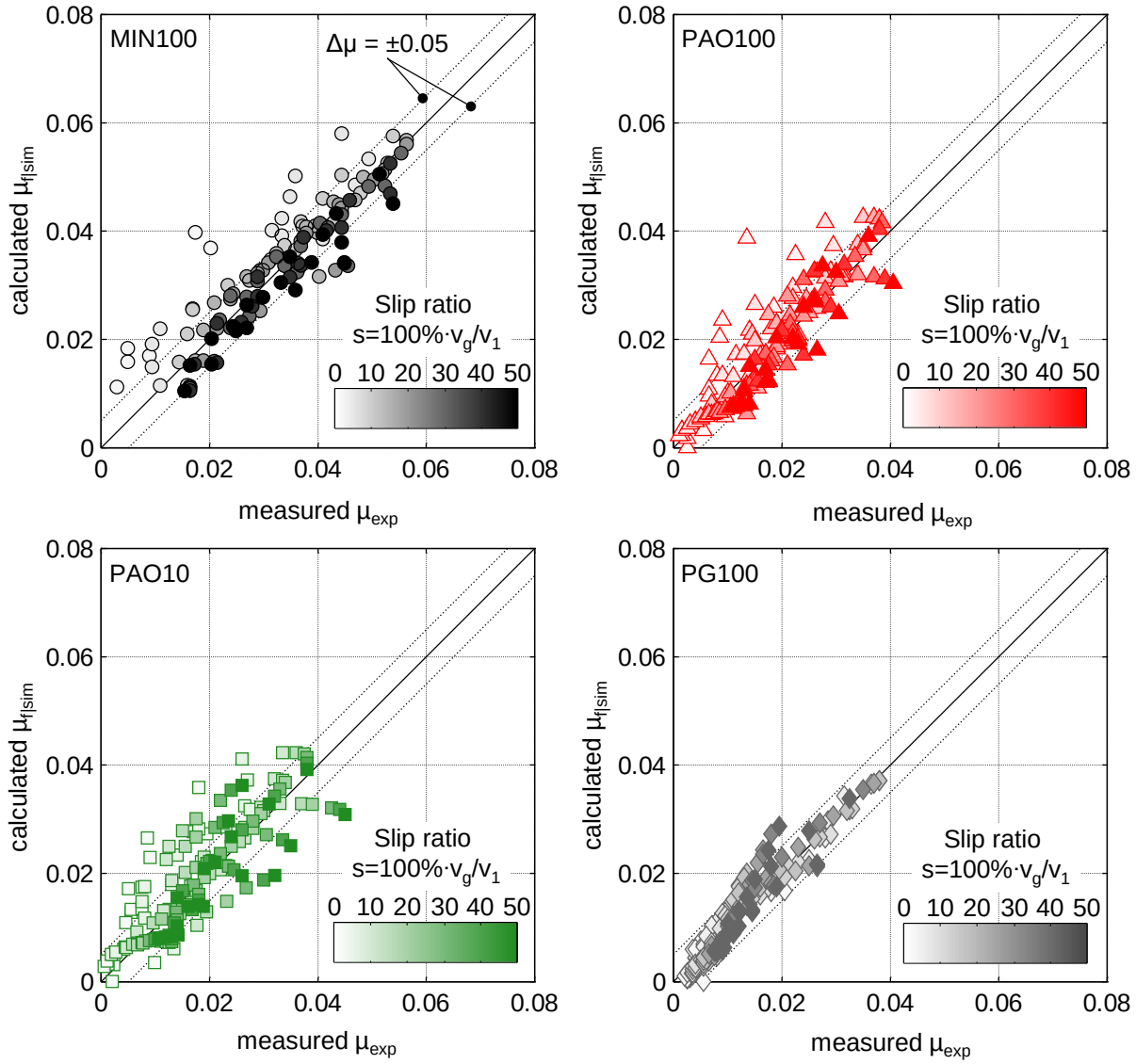

Figure 7: Comparison of simulated ($\mu_{f|sim}$) and measured (μ_{exp}) coefficients of friction for all operating conditions and for lubricants MIN100, PAO10, PAO100 and PG100 (measured data acc. to Mayer [22])

5 CONCLUSION

This paper focuses on a limiting shear stress formulation for use in TEHL simulation models. The main conclusions drawn from this work are:

- Non-Newtonian fluid models based on limiting shear stress are currently probably the most physical and suitable way to calculate the friction of TEHL contacts.
- The limiting shear stress is not a constant lubricant property but depends on pressure, temperature, entrainment velocity and type of lubricant.
- The contact-integral nature of limiting shear stresses derived from friction measurements at tribometers has been successfully adjusted for local use in TEHL simulation models.

- The presented contact-local limiting shear stress formulation is transferable to other tribological systems apart from the twin disk test rig e.g. gear contacts.
- TEHL simulation results show very good agreement between measured and simulated coefficients of friction for a large variety of operating conditions and lubricants.
- When the sliding velocity is increased further once the maximal friction is reached, the portion of friction reduction due to decreasing lubricant viscosity and the portion due to temperature dependency of the limiting shear stress have been quantified.

Further work might focus (i) on even extending the data basis for the contact-integral limiting shear stress equation, (ii) on accurate modelling of the beginning of the friction curves at the non-linear (shear thinning) transition regime, and (iii) on the transition of the calculated contact-local limiting shear stress $\tau_{lim\,|sim}$ to the minimum limiting shear stress $\tau_{lim,m}$.

NOMENCLATURE

A_H	Hertzian flattening area	x	Film thickness length direction
$c_{p,f}$	Specific heat capacity of lubricant	z	Film thickness height direction
$E_{\dot{\gamma}1}$, $E_{\dot{\gamma}2}$, $E_{\dot{\gamma}3}$, $E_{\dot{\gamma}4}$	Lubricant specific parameters of $\tau_{lim\,|exp}$	z_η	Pressure exponent of Roelands equation
F_N	Normal force	α_p	Pressure-viscosity exponent
F_R	Friction force	$\dot{\gamma}_{fzx}$	Simulated shear rate
G	Shear modulus of lubricant	η	Dynamic viscosity
h	Lubricant film thickness	ϑ_M	Bulk temperature in °C
l_{eff}	Effective contact width	ϑ_{Oil}	Oil inlet temperature in °C
p	Pressure	λ_f	Thermal conductivity of lubricant
p_H	Hertzian pressure	μ_{exp}	Measured coefficient of friction
p_m	Mean Hertzian pressure ($= \pi/4 \cdot p_H$)	$\mu_{f\,|sim}$	Simulated coefficient of friction
s	Slip ratio ($= 100\% \cdot v_g/v_1$)	ν	Kinematic viscosity
T	Temperature in K	ρ_f	Density of lubricant
T_M	Bulk temperature in K	τ_{fzx}	Simulated shear stress
T_{Oil}	Oil inlet temperature in K	$\tau_{lim\,|exp}$	Contact-integral limiting shear stress
T_{ref}	Reference temperature in K	$\tau_{lim\,|sim}$	Contact-local limiting shear stress
v_g	Sliding velocity ($= v_1 - v_2$)	$\tau_{lim\,|m}$	Minimum limiting shear stress
v_Σ	Sum velocity ($= v_1 + v_2$)		

REFERENCES

[1] Bair, S.: A Rough Shear-Thinning Correction for EHD Film Thickness. Tribology Transactions 47(3): pp. 361-365 (2004).

[2] Bair, S.: High Pressure Rheology for Quantitative Elastohydrodynamics. 1st Edition, Amsterdam: Elsevier (2007).

[3] Bair, S.: The Nature of the Logarithmic Traction Gradient. Tribology International 35: pp. 591-597 (2002).

[4] Bair, S.; McCabe, C.: A Study of Mechanical Shear Bands in Liquids at High Pressure. Tribology International 37: pp. 783-789 (2004).

[5] Bair, S.; Vergne, P.; Kumar, P.; Poll, G.; Krupka, I.; Hartl, M.; Habchi, W.; Larrson, R.: Comment on „History, Origins and Prediction of Elastohydrodynamic Friction“ by Spikes and Jie. Tribology Letters 58(16): pp. 1-8 (2015).

[6] Bair, S.; Winer, W. O.: A Rheological Model for Elastohydrodynamic Contacts based on Primary Laboratory Data. ASME Journal of Lubrication Technology 101: pp. 258-265 (1979).

[7] Bair, S.; Winer, W. O.: Some Observations in High Pressure Rheology of Lubricants. Journal of Lubrication Technology 104: pp. 357-364 (1982).

[8] Bair, S.; Winer, W. O.: The High Pressure High Shear Stress Rheology of Liquid Lubricants. Journal of Tribology 114: pp. 1-9 (1992).

[9] Bartel, D.: Simulation von Tribosystemen: Grundlagen und Anwendungen. Habilitationsschrift. 1st Edition, Wiesbaden: Vieweg+Teubner (2009).

[10] Beilicke, R.; Bobach, L.; Bartel, D.; Bader, N.; Poll, G.; Brouwer, L.; Schwarze, H.: Tribologische Fluidmodelle zur Simulation der Reibung in geschmierten konzentrierten Kontakten. 56. GfT-Tribologie-Fachtagung, Göttingen, pp. 5/1-5/14 (2015).

[11] Bobach, L.; Bartel, D.; Beilicke, R.; Mayer, J.; Michaelis, K.; Stahl, K.; Bachmann, S.; Schnagl, J.; Ziegele, H.: Reduction in EHL Friction by a DLC Coating. Tribology Letters 60(17): pp. 1-13 (2015).

[12] Bode, B.: Modell zur Beschreibung des Fließverhaltens von Flüssigkeiten unter hohem Druck. Tribologie und Schmierungstechnik 36: pp. 182-189 (1989).

[13] Evans, C. R.; Johnson, K. L.: The Rheological Properties of Elastohydrodynamic Lubricants. Journal of Mechanical Engineering Science 200(5): pp. 303-312 (1986).

[14] Eyring, H.: Viscosity, Plasticity, and Diffusion as Examples of Absolute Reaction Rates. Journal of Chemical Physics 4(4): pp. 283-291 (1936).

[15] Fulcher, G. S.: Analysis of Recent Measurements of the Viscosity of Glasses II. Journal of the American Ceramic Society 8(12): pp. 789-794 (1925).

[16] Habchi, W.: A Full-System Finite Element Approach to Elastohydrodynamic Lubrication Problems: Application to Ultra-Low-Viscosity Fluids. Dissertation. L’Institut National des Sciences Appliquées, Lyon (2008).

[17] Habchi, W.; Bair, S.; Vergne, P.: On Friction Regimes in Quantitative Elastohydrodynamics. Tribology International 58: pp. 107-117 (2013).

[18] Hepermann, P.; Beilicke, R.; Bartel, D.; Tenberge, P.; Deters, L.: AiF-Nr. 16057, FVA-Nr. 598/I - Heft 1024 - Örtliche Fresstragfähigkeit Abschlussbericht - Bestimmung der örtlichen Fresstragfähigkeit: Einfluss von Schräg- und Hochverzahnungen. Forschungsvereinigung Antriebstechnik e.V., Frankfurt/Main (2012).

[19] ITR Clausthal: IGF-Nr. 15786 N, FVA-Nr. 583/I - Heft 1002 - Thermophysikalische Eigenschaften (Schmierstoffe) - Bestimmung und Modellierung der thermophysikalischen Eigenschaften von Schmier- und Kraftstoffen unter hohen Drücken. Forschungsvereinigung Antriebstechnik e.V., Frankfurt/Main (2013).

[20] Larsson, R.; Andersson, O.: Lubricant Thermal Conductivity and Heat Capacity under High Pressure. Journal of Engineering Tribology 214 (4): pp. 337-342 (2000).

[21] Lohner, T.; Ziegltrum, A.; Stemplinger, J.-P.; Stahl, K.: Engineering Software Solution for Thermal Elastohydrodynamic Lubrication (TEHL) Using Multiphysics Software. Advances in Tribology. Article ID 6507203: doi: 10.1155/2016/6507203, 13 pages (2016).

[22] Mayer, J.: Einfluss der Oberfläche und des Schmierstoffs auf das Reibungsverhalten im EHD-Kontakt. Dissertation. Technical University of Munich (2013).

[23] Paschold, C.: Ableitung eines Grenzschubspannungsansatzes für Schmierstoffe auf Basis experimenteller Untersuchungen am Zweischeibenprüfstand. Semester Thesis, Institute of Machine Elements, Technical University of Munich (2015).

[24] Research Project FVV 1138: Tribologische Fluidmodelle. Research Association for Combustion Engines e. V. (FVV e. V.). Funded via the German Federation of Industrial Research Associations e. V. (AiF e. V.) by the German Federal Ministry for Economic Affairs and Energy (BMWi).

[25] Roelands, C. J. A.: Correlation Aspects of the Viscosity-Temperature Relationship of Lubricating Oil. Dissertation. Delft University of Technology (1966).

[26] Tammann, G.; Hesse, W.: Die Abhängigkeit der Viskosität von der Temperatur bei unterkühlten Flüssigkeiten. Z. f. anorg. u. allg. Chemie 156: pp. 245-257 (1926).

[27] Vogel, H.: Das Temperaturabhängigkeitsgesetz der Viskosität von Flüssigkeiten. Physik. Zeitschrift 22: pp. 645-647 (1921).

[28] Wolff, R.; Kubo, A.: A Generalized Non-Newtonian Fluid Model Incorporated Into Elastohydrodynamic Lubrication. Journal of Tribology 118(1): pp. 74-82 (1996).